Laser-induced photochemistry of methane on Pt(111): Excitation mechanism and dissociation dynamics

Yoshiyasu Matsumoto, Yuri A. Gruzdkov,[a] Kazuo Watanabe, and Kyoichi Sawabe
Institute for Molecular Science, Myodaiji, Okazaki, 444 Japan

(Received 31 July 1995; accepted 11 June 1996)

Adsorption states and photochemistry of methane and deuterated methane on a Pt(111) surface have been investigated by measuring temperature-programmed desorption spectra, x-ray photoelectron spectra, work function changes, and angle-resolved time-of-flight distributions of desorbed species. Methane weakly adsorbed on the Pt(111) surface at 40 K is dissociated to methyl and hydrogen fragments with laser irradiation at 193 nm. This is remarkably different from the photochemistry of methane in the gas phase where photodissociation takes place only at $\lambda<145$ nm. While the photofragments mostly remain on the surface, some fraction of methyl desorbs with average translational energy of 0.27 eV. Photodesorption of methane is a minor channel. Desorbed methane is sharply collimated along the surface normal and shows two hyperthermal velocity components. Among the two, the faster component is attributed to associative recombination between a methyl adsorbate and a hydrogen atom produced by the photodissociation of adsorbed methane. The photochemical processes are substantially suppressed when the surface is covered with methyl adsorbate of 0.14 ML achieved by an extensive irradiation of 193-nm photons. In contrast, no photochemical reactions result from the 193-nm irradiation of methane adsorbed on a Xe/Pt(111) overlayer or from the 248-nm irradiation of methane on the bare Pt surface. These results indicate that the photochemical processes occur only for methane in close contact with substrate atoms under the irradiation of 193-nm photons. The incident angle dependence of cross sections of the photochemistry obtained with linearly polarized light indicates that direct electronic excitation of methane adsorbate plays an important role in the photochemistry of methane. The photochemistry of methane on Pt(111) at the wavelength substantially longer than that in the gas phase implies that the electronic excited state of methane is significantly mixed with substrate electronic states. [S0021-9606(96)01435-3]

I. INTRODUCTION

Photon irradiation onto adsorbates on solid surfaces provides a good opportunity for exploring various nonthermal processes induced by electronic transitions of adsorbates. One of the interesting questions on photo-induced processes is how nuclear dynamics proceeds on relevant potential energy surfaces (PES). Although surface photochemistry on well-defined surfaces is relatively a new field, a large number of studies have been reported in recent years.[1–5] However, more extensive theoretical and experimental studies are required for detailed understandings of the dynamics, since excitation mechanisms and relevant excited states are not necessarily clear. Thus, a central and fundamental question on this subject is to clarify how adsorbate–substrate systems are excited with photon irradiation.

Two different excitation mechanisms have been frequently discussed: (1) indirect excitation via substrate-mediated charge transfer and (2) direct excitation within adsorbate. In the former mechanism electrons or holes created by photon absorption of metal and semiconductor substrates are attached resonantly to adsorbates. If photo- and/or ''hot'' electrons are attached to adsorbates, transiently formed negative ions lead to desorption or dissociation of the adsorbates. This mechanism is widely believed to be very important in photochemistry on metal and semiconductor surfaces under the irradiation of UV photons <7 eV. In the latter mechanism, the electronic excitation is localized at an adsorbate. This is essentially the same excitation mechanism as that in isolated atoms and molecules in the gas phase.

These excitation mechanisms are two extreme cases in surface photochemistry. In reality, the electronic states of adsorbates and substrates cannot be treated independently, since they interact with each other. If adsorbate–substrate interactions are strong, it is more reasonable to think of an adsorbate–substrate complex. One can draw an analogy between electronic excitation in organometallic compounds and that in the adsorbate–substrate complex. However, it should be noted that adsorbates interact with substrate continuum orbitals, while ligands interact with discrete orbitals centered on a metal atom.[5] Thus, the strong adsorbate–substrate interactions make it difficult to distinguish ''metal-to-ligand charge transfer'' excitation in the adsorbate–substrate complex from the substrate-mediated charge transfer excitation.

In this regard, photochemistry of physisorbed molecules on metal surfaces provides a unique opportunity for understanding the excitation mechanism. Since the adsorbate weakly interacts with the surface, one might think intuitively that the electronic structure of the adsorbate is not quite dif-

[a]Present address: Shock Dynamics Center, Washington State University, Pullman, Washington 99164-2814.

ferent from that in the gas phase. In other words absorption bands will not show a large shift when molecules are physisorbed on the surface. Thus, one might be able to sort out excitation mechanisms by observing photochemistry at photon energy on and out of resonance of intra-adsorbate electronic excitation. This is indeed the case for adsorbates on dielectric surfaces.[3] However, is it also true for those on metal surfaces? In this paper, we focus on the question dealing with a specific adsorption system, i.e., methane on Pt(111).

We have reported that methane weakly adsorbed on Pt(111) can be readily dissociated to produce methyl and hydrogen adsorbates upon irradiation with 193-nm (6.4 eV) photons.[6] The evidence has also been confirmed by infrared reflection-absorption spectroscopy (IRAS).[7] Methane weakly adsorbs on Pt(111). The activation energy for desorption is 0.23 eV. Since methane in the gas phase does not show any appreciable absorption cross sections above 145 nm,[8–10] it is transparent at 193 nm. Thus, the intuition cited above makes it difficult to expect that the direct excitation takes place at 193 nm. This prompts us to favor the indirect excitation mechanism. However, the substrate-mediated electron transfer excitation is also difficult to realize in the following reason. The negative ion state leading to dissociative electron attachment (DEA), $e + CH_4 \rightarrow (CH_4^-)^{\ddagger} \rightarrow CH_3 + H^-$, is also located at high energy; the DEA cross section of the gaseous methane has the threshold at 7 eV and shows a double-humped feature peaked at 9.2 and 10.2 eV.[11] Irradiation of 6.4-eV photons onto a Pt(111) surface produces photoelectron whose kinetic energy is 0.6 eV at most. Thus, even if the negative ion states were stabilized by the image-charge interaction and so forth, these states could be hardly reached by the photoelectrons. Therefore, the excitation mechanism in the photochemistry of methane on Pt(111) is really puzzling. To obtain more insight on the excitation mechanism, we have recently measured how cross sections of the photochemical processes depend on the incident angle of light with fixed linear polarization.[12] This measurement clearly demonstrates that direct excitation plays an important role.

In this paper we describe a detailed study on the adsorption of methane on Pt(111), the excitation mechanism and dynamics of its photochemical processes induced by UV laser irradiation. In Sec. III A, the adsorption states of methane are characterized by temperature-programmed desorption (TPD), x-ray photoelectron spectroscopy (XPS), and work function measurements. In Secs. III B and III C, the photochemical processes of methane at a bare Pt(111) surface and on a Xe overlayer are investigated mainly with post-irradiation TPD and XPS. In Sec. III D, desorption dynamics is studied by angle-resolved time-of-flight (TOF) measurements of desorbed species. In Sec. III E, polarization-dependent photochemical cross sections are measured as a function of incident angles. In Sec. IV, plausible excitation mechanisms are discussed on the basis of the obtained results and the electronic structure of methane in the gas phase.

II. EXPERIMENT

The experiments reported here were performed in an ultrahigh vacuum apparatus (base pressure $\leqslant 1\times10^{-10}$ Torr) that has been described in detail elsewhere.[13,14] Briefly, it is evacuated by cascaded turbomolecular pumps and equipped with a four-grids retardation electron analyzer for low energy electron diffraction (LEED), Auger electron spectroscopy, an x-ray gun and a hemisphere electron energy analyzer for XPS, a differentially pumped quadrupole mass spectrometer (QMS), an ion gun, a high precision sample manipulator, and laser inlet/outlet ports with CaF_2 windows.

A Pt(111) crystal with dimensions of 10 mm (diameter) $\times$1.0 mm (thickness) was cleaned by the conventional treatment: the repeating of many cycles of Ar^+ sputtering, prolonged heating at 800 K in 1×10^{-7} Torr oxygen, and annealing at 1200 K. The sample was mounted between a pair of tantalum wires that were connected via a massive copper block to a closed-cycle He refrigerator. The sample was electrically isolated by thin sapphire cylinders inserted in between the copper block and the wires holding the sample. The lowest surface temperature was 40 K and the sample could be resistively heated above 1200 K. The crystal temperature was monitored with a Chromel–Alumel thermocouple spot-welded to the edge of the crystal.

Exposures of CH_4 or CD_4 were carried out at the surface temperature of 55 K to make a saturated first layer or at 40 K to make multilayers. Normally, 2.0 L (1 L$=10^{-6}$ Torr s) exposure at 55 K was used to make a perfectly saturated first layer of methane. The absolute coverage of methane was determined by comparing XPS spectra of C($1s$) of methane with those of CO. Adsorbed states of methane were characterized by TPD, XPS, and work function changes. For TPD measurements the sample was positioned at 1 mm off the skimmer of the QMS chamber; this minimizes spurious contributions originating from a sample mount and a rear side of the crystal. Changes in the work function of Pt(111) were measured as a function of methane coverage by monitoring a cutoff edge of secondary electrons induced by x-ray irradiation (Mg-$K\alpha$). In these measurements the sample was biased at -25 V.

Unless noted specifically, nonpolarized ultraviolet light from an excimer laser (ArF: 193 nm, and KrF: 248 nm) was directed onto the surface at 40 K. The laser beam was expanded with a beam expander for irradiating the entire surface uniformly. Laser pulses (2 mJ/cm^2, 15 ns) at the repetition rate of 5 Hz did not raise time-averaged surface temperature over 50 K during photon irradiation. The maximum transient temperature jump due to pulse-laser heating was estimated to be 7 K (Ref. 15) at the incident angle of 0°, which does not exceed the desorption temperature (see below). Thus, thermal effects were negligible. For measurements of the polarization-dependent cross sections of the photochemical processes, the incident light was polarized with a polarizer composed of five pairs of UV-grade fused quartz plates placed at the Brewster angle at 193 nm.

Post-irradiation TPD and XPS were used to quantify the photodissociated fraction of methane as a function of the

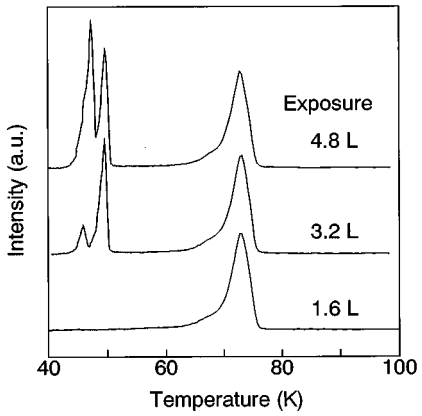

FIG. 1. A series of TPD spectra of CH_4 from Pt(111) as a function of exposure. The surface was exposed to methane at 40 K. Signals were detected at $m/e=13$ (CH^+). The heating rate was 0.3 K s^{-1}. The desorption peak at 73 K is due to methane from the first layer and the peaks around 50 K are from multilayers.

number of accumulated photons incident on the unit surface area, N_{ph}. Standard cleaning and annealing cycles were necessary after each photolysis experiment owing to the accumulation of small amounts of carbon supplied from photofragments of methane adsorbates.

TOF distributions of desorbed species were measured at various desorption angles. The surface was first saturated with methane at 55 K and then 193-nm excimer laser pulses were directed to the surface at 40 K. Desorbed species were detected by the QMS and the signals were accumulated on a multichannel scaler. The ionizer of the QMS was located at 23 cm from the surface. The ion flight time in the QMS was separately determined and subtracted from the measured flight time. For angular distribution measurements of desorbed species, the number of accumulated photons was kept constant, i.e., 5.2×10^{18} cm^{-2} at each desorption angle.

III. RESULTS AND INTERPRETATION

A. Adsorption state

Figure 1 shows a series of TPD results of methane on Pt(111) measured at $m/e=13$ (CH^+). Signals detected at the other mass numbers due to the cracking of methane in the QMS ionizer gave essentially identical TPD results. A desorption peak at 73 K increases with exposure and then saturates around 1.6 L at 40 K. With more extensive exposures, new desorption peaks originating from physisorbed multilayers of methane appear at 46, 48, and 50 K. These features are in good agreement with those reported previously.[16,17] TPD results of CD_4 as a function of exposure were identical with those of CH_4 except that a slightly higher exposure was needed to make overlayers of CD_4.

Further annealing to higher temperatures did not give any desorption peaks. The C(1*s*) peak of CH_4 at 283.5 eV was completely depleted after the TPD measurement. Thus, all of the methane adsorbates desorb molecularly and do not dissociated thermally. This is consistent with the results in molecular beam studies[18,19] showing that hyperthermal kinetic energy of incoming methane is needed for dissociative chemisorption on Pt(111).

The desorption peak at 73 K was analyzed with the first order desorption kinetics, i.e., $-d\theta_\alpha/dt=\theta_\alpha\nu\times\exp(-E_a/kT)$, where θ_α is the coverage of methane, E_a an activation energy, and ν a pre-exponential factor. Since E_a and ν generally depend on adsorbate coverage, the fitting of the TPD peak was limited to a small threshold region at the onset of desorption so that θ_α decreases no more than a few percent of its initial value.[20] This analysis gave $E_a=0.23$ eV and $\nu=2\times10^{16}$ s^{-1} and indicated a slight activation energy increase ($\sim$0.065 eV) with decrease of initial coverage down to 25% of the saturation coverage. The small activation energy for desorption indicates that methane interacts with the substrate weakly. Its decline with the increase of coverage suggests a slightly repulsive mutual interaction of methane adsorbates within the first layer.

Although LEED observations were attempted as a function of methane coverage up to the saturation, no LEED patterns were observed. This indicates that methane adsorbates do not have a long range order. However, note that electrons with the kinetic energy of $\sim$50 eV may easily stimulate desorption of the weakly bound adsorbates during the LEED observations. Thus, this made it difficult to ensure a long range order of methane adsorbates in the first layer if it is possible at all.

The absolute coverage of methane was calibrated by comparing integrated areas of the C(1*s*) peak of CO adsorbed on Pt(111). The saturation coverage of CO on Pt(111) at 300 K was reported to be 0.5 ML.[21] Here ML is defined as the coverage referenced to the Pt atom number density in the topmost layer. This was confirmed in the following way. First, under this dosing condition a sharp $c(4\times2)$ LEED pattern was observed, which is indicative of this coverage. Second, the integrated area of a double-peaked O(1*s*) line of CO was exactly twice as large as that of 0.25 ML-oxygen adatoms with a $p(2\times2)$ structure. Some complication arises in this approach since the C(1*s*) peak of CO shows an extended region of shake-up intensity about 9 eV wide on the high binding energy side of the main peak.[22] This region gains a considerable fraction of the total intensity of the C(1*s*) peak. In contrast, no shake-up satellites were observed for the C(1*s*) peak of methane. The ratio of the C(1*s*) peak area of saturated CH_4 to that of 0.5 ML CO was calculated to be 0.67 ± 0.10 and therefore the absolute saturation coverage of CH_4 was determined to be 0.33 ± 0.05 ML. The relatively large experimental error is due to some uncertainty in setting the upper limit for integration of the shake-up region. The saturation coverage of CD_4 was measured to be the same as for CH_4.

Figure 2 shows work function changes of the Pt(111) surface as a function of methane coverage. If the adsorbate-induced surface-potential change is caused by the sum of dipoles at the surface, the work function change, $\Delta\phi$, is proportional to the dipole moment, d_0, of the individual absorption complex and the number of adsorbed molecules per surface area, $n_{\mathrm{ad}}(=1.5\times10^{19}\theta_\alpha\ \mathrm{m}^{-2})$,

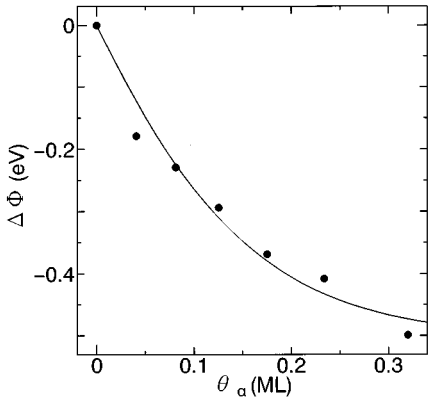

FIG. 2. Changes in the work function of Pt(111), $\Delta\phi$, as a function of the coverage of methane, θ_α. A solid curve was a result of fitting to the Topping model.

$$\Delta\phi = -4\pi f^* d_0 n_{\mathrm{ad}}, \tag{1}$$

where $f^* = (4\pi\epsilon_0)^{-1}$. However, the work function of Pt(111) first decreases rapidly with increasing methane coverage (0–0.04 ML), then decreases more slowly at high coverages (0.04–0.33 ML). The slow decrease of $\Delta\phi$ at the high coverages indicates that depolarization effects due to lateral interactions among adsorbate dipoles play a role. The depolarization effects can be accounted for by the Topping formula,[23]

$$\Delta\phi = -4\pi f^* d_0 n_{\mathrm{ad}}(1+9\alpha n_{\mathrm{ad}}^{3/2})^{-1}, \tag{2}$$

where α is the polarizability of the adsorbate. Fitting to the formula yielded the dipole moment per a methane adsorbate to be 0.54 D (1 D$=3.3\times10^{-30}$ A s m) at the limit of $\theta_\alpha \rightarrow 0$.

B. Photochemistry at clean Pt(111)

Photochemistry of methane adsorbates was studied by post-irradiation TPD and XPS. The surface was first saturated with methane to form a monolayer and then irradiated with 6.4-eV photons at the surface temperature of 40 K. For comparison, a TPD result before laser irradiation is again depicted in the top trace of Fig. 3; only the molecular desorption peak denoted as α was observed. In contrast to the preirradiation TPD result, the post-irradiation TPD result depicted in the middle trace shows that the α-desorption peak is depleted, shifted by a few degrees to the lower temperature and develops a shoulderlike peak at around 55 K. These features became more and more prominent with the increasing number of photons accumulated. Moreover, another striking feature in the post-irradiation TPD result is that a new peak denoted as β at around 260 K appears; its intensity also depends on the number of accumulated photons.

It has been reported that methane desorption at 240–280 K is attributable to the associative recombination of CH_3 and H.[17,24–26] Thus, the appearance of the β peak strongly suggests that CH_3 and H adsorbates are present after irradiation. If this is so, hydrogen–hydrogen recombination and methyl dehydrogenation channels may also take place in addition to the recombination of CH_3 and H. Thus, detection of H_2 desorption would provide another piece of evidence for photodissociation of methane. Unfortunately, our apparatus does not allow us to measure TPD spectra at $m/e=2$ because large background signals originated from residual hydrogen gas in the QMS chamber. Thus, we obtained the necessary evidence by carrying out the same experiment with deuterated methane.

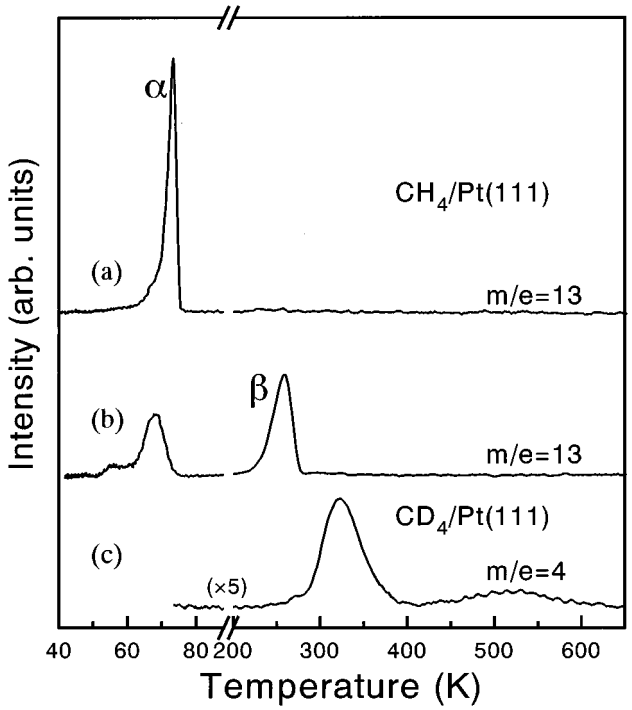

FIG. 3. TPD spectra of methane ($m/e=13$) (a) before and (b) after irradiation of 6.4-eV photons derived from Pt(111) saturated with CH_4. The TPD spectra of CD_4 (not shown) are basically identical to those of CH_4. (c) Post-irradiation TPD spectrum of D_2 ($m/e=4$) from Pt(111) saturated with CD_4. The surface was first exposed to CH_4 (CD_4) at 40 K. The number of accumulated photons was 5.6×10^{18} cm^{-2}. The heating rates were 0.3 and 5.0 K s^{-1}, below and above 164 K, respectively.

Post-irradiation TPD spectra detected at $m/e=20$ (CD_4^+) were essentially the same as those of CH_4. The bottom trace of Fig. 3 shows a post-irradiation TPD result detected at $m/e=4$. Indeed, D_2 desorption peaks were detected at 320 and 520 K. The first peak is attributable to deuterium-atom recombination while the second one to dedeuteration of CD_3 adsorbates.[25,26] *Therefore, these results clearly indicate that methane adsorbed on Pt(111) is dissociated with the irradiation of 6.4-eV photons to produce methyl and hydrogen atom adsorbates on the surface*. This conclusion has also been confirmed recently by post-irradiation IRAS, which identified CH_3 adsorbates produced by the irradiation of 6.4-eV photons.[7]

Post-irradiation C($1s$)-XPS spectra are shown in Fig. 4. Before irradiation a single Gaussian-shaped peak was observed at the binding energy of 283.5 eV. After irradiation the intensity decreased and the maximum position shifted by ~0.1 eV towards the higher binding energy. When the surface was annealed to 80 K after irradiation the C($1s$) peak is shifted in the opposite direction to 282.7 eV and became

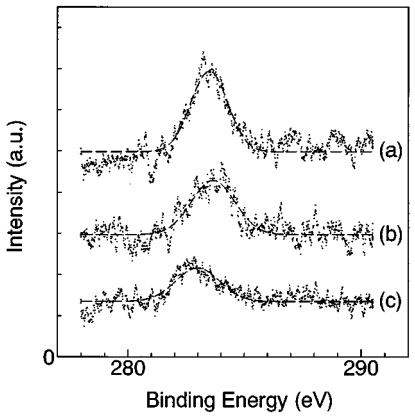

FIG. 4. A series of C(1*s*) XPS spectra before and after irradiation with 6.4-eV photons. The surface was first saturated with methane. The spectra were taken (a) before irradiation, (b) after irradiation of 6.4-eV photons, and (c) further annealing to 80 K. Since methane is desorbed by the annealing process, the spectrum (c) represents the C(1*s*) peak of methyl adsorbates produced by photodissociation of methane.

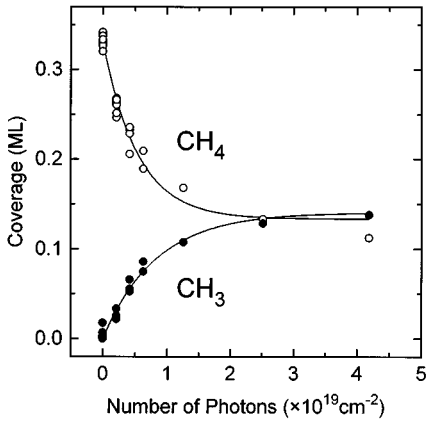

FIG. 5. Plots of the coverages of methane (open circle) and methyl (solid circle) adsorbates as a function of the number of accumulated 6.4-eV photons. The surface was first saturated with methane at 40 K and irradiated with 6.4-eV photons along the surface normal. The solid curves show the results of least-squares fittings to Eqs. (3) and (4).

slightly asymmetric. Since unreacted methane is desorbed by the annealing procedure, the peak is attributed to strongly bound adsorbates. Combining with the TPD results we assign the peak at 282.7 eV to methyl adsorbate on Pt(111).

The annealing procedure to 80 K after irradiation served to measure C(1*s*) signal intensities of methane and methyl adsorbates separately. Having established a linear relationship between the coverage of methane and the signal intensity of the C(1*s*) peak, we applied this relationship to methyl adsorbate to estimate its coverage. The XPS data were used for determining the methyl coverage only when it was relatively large to give reasonable S/N ratios in the spectra. When methyl coverage was small, large errors in coverage estimation were introduced mainly in the process of base line subtraction. Thus, we instead used β-desorption peaks to estimate methyl coverage in the low coverage range after having established a linear relationship between the integrated area of the methyl C(1*s*) peak and that of the β-desorption peak in the high coverage range. With this method, the area of the β-desorption peak might be affected by the side channels of H and CH_3 consumption, i.e., hydrogen atom recombination and dehydrogenation of methyl adsorbates during the annealing procedure of TPD as mentioned earlier. However, we confirmed that these channels are insignificant, since the amount of hydrogen desorption in the TPD measurements is estimated to be less than a few percent of the entire amount of hydrogen atoms produced by irradiation up to $N_{\mathrm{ph}}=5.5\times10^{19}$ cm^{-2}. In addition, XPS data confirmed that the amount of carbon remained on the surface after TPD is only a few percent of the initial methane coverage. Thus, this calibration procedure would underestimate the absolute coverage of methyl adsorbates by 4% at most.

Figure 5 shows how the coverages of methane and methyl adsorbates, θ_α and θ_β, respectively, change as a function of the number of accumulated photons incident on the unit area of the substrate, N_{ph}. The data were deduced from the integrated areas of both α- and β-desorption peaks, and the C(1*s*) peak areas of each species as alluded above. The coverage of methane decreases with N_{ph}, but that of methyl increases. However, note that the depletion of θ_α significantly slows down and θ_β becomes almost constant at 0.14 ML when N_{ph} exceeds over 2×10^{19} cm^{-2}. This indicates that a self-quenching mechanism for the photochemistry takes place when the surface is covered with methyl and hydrogen adsorbates. Since we have confirmed that the photochemistry of methane takes place on a Pt(111) saturated with hydrogen adatoms,[27] methyl adsorbates play a major role in the self-quenching mechanism. At $N_{\mathrm{ph}}=4.5\times10^{19}$ cm^{-2} the loss in θ_α is 0.19 ML that exceeds over the gain in θ_β, i.e., 0.14 ML. This discrepancy indicates that other photochemical processes such as photodesorption of methane also take place.

We attempted to detect ethane and ethylene desorbed from the surface during 6.4-eV photon irradiation by measuring signals at $m/e=30$ ($C_2H_6^+$) and 27($C_2H_3^+$). However, signals were all below the detection limit. Thus, C–C coupling does not take place photochemically. Those molecules were not detected either in post-irradiation TPD after the surface was irradiated with the accumulated number of photons $N_{\mathrm{ph}}=4\times10^{19}$ cm^{-2}. This implies that the associative recombination of methane is a dominant thermal process and C–C coupling reactions are negligible in the Pt(111) surface covered with CH_3, H, and unreacted methane.

The decay and the rise of adsorbate coverage in the coverage- N_{ph} curves give a quantitative measure for the photochemical processes. Least-squares fits were made by using the following equations obtained under simple first-order kinetics:

$$\theta_\alpha(N_{\mathrm{ph}})=[\theta_\alpha(0)-\theta_\alpha(N_{\mathrm{ph}}^f)]\exp(-\sigma_\alpha N_{\mathrm{ph}})+\theta_\alpha(N_{\mathrm{ph}}^f), \tag{3}$$

$$\theta_\beta(N_{\mathrm{ph}})=\theta_\beta(N_{\mathrm{ph}}^f)[1-\exp(-\sigma_\beta N_{\mathrm{ph}})], \tag{4}$$

where σ_i's ($i=\alpha,\beta$) are effective cross sections obtained from α- and β-desorption peaks, respectively, and $\theta_i(N_{\mathrm{ph}}^f)$ the coverage of adsorbates at $N_{\mathrm{ph}}=4.2\times10^{19}$ cm^{-2}. If there

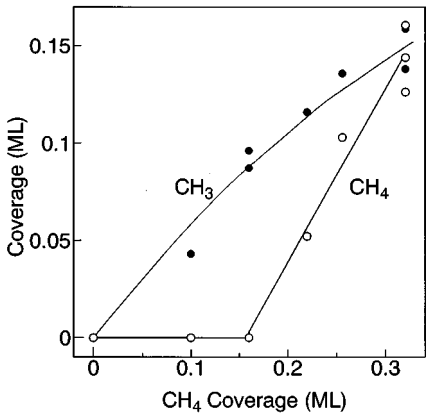

FIG. 6. Plots of final coverages of methane (open circle) and methyl (solid circle) as a function of the initial coverage of methane on Pt(111). The number of accumulated photons at 193 nm was 4.7×10^{19} cm^{-2}, which is enough to reach the saturation region where the adsorbate coverages become constant.

were no loss mechanisms for produced methyl adsorbates during photon irradiation, $\sigma_\alpha=\sigma_\beta$. Fitting these data to the equations with a common free parameter of σ yields σ to be 1.5×10^{19} cm^2 for the saturation coverage of methane. However, there is a loss mechanism of CH_3 adsorbate as described in Sec. III D. Thus, when the fittings are made for θ_α and θ_β independently, $\theta_\alpha(N_{\rm ph})$ gives $\sigma_\alpha=1.9\times10^{-19}$ cm^2 and $\theta_\beta(N_{\rm ph})$ gives $\sigma_\beta=1.2\times10^{-19}$ cm^2.

Figure 6 shows how photoyields depend on the initial coverage of methane, $\theta_\alpha(0)$. Here, the coverages of CH_3 and CH_4 after the methane-covered Pt(111) surface was irradiated by 6.4-eV photons of $N_{\rm ph}=4.7\times10^{19}$ cm^{-2} as a function of $\theta_\alpha(0)$. The amount of leftover methane decreases almost linearly to the vanishing point at 0.16 ML initial coverage. In other words adsorbed methane can be completely depleted when the initial coverage is below one-half of the saturation coverage. A number of produced methyl adsorbates also decreases monotonically with the decreasing of the initial methane coverage.

To examine whether the photochemical processes are induced by multiphonon excitation, we changed the fluence of individual laser pulses from 1 to 10 mJ cm^{-2}, corresponding to the change in the peak intensity of laser pulses from 67 to 670 kW cm^{-2}, while keeping $N_{\rm ph}$ constant at 3.6×10^{18} cm^{-2}. Post-irradiation TPD results were essentially identical within each set of experiments. This proves that the photoreaction rate is indeed proportional to the light intensity and multiphoton excitation is not likely responsible for the photochemistry.

Photochemistry of methane under the irradiation of 248-nm (5.0 eV) photons was also examined. The Pt(111) saturated with CH_4 was irradiated with 5.0-eV photons. No detectable β peak of methane was observed with prolonged irradiation up to $N_{\rm ph}=3.2\times10^{20}$ cm^{-2}. Post-irradiation XPS showed that the depletion of the C($1s$)-peak intensity is negligible. When a substantially high laser fluence of 12.5 mJ cm^{-2} was used, the α peak was depleted by about 50% with the prolonged irradiation. The TOF measurement of methane under the irradiation condition indicated that this depletion is due to methane desorption induced by thermal heating; a TOF distribution is composed of a slow velocity component with the translational temperature, $\langle E_T\rangle/2k=87$ K, which is close to the estimated transient surface temperature of 90 K. These results made us to conclude that *no photodissociation and photodesorption of methane take place under the irradiation of 5.0-eV photons.*

C. Photochemistry on a Xe overlayer

In this section we describe a set of experiments undertaken to study the photochemistry of methane separated by a spacer of photochemically inert substance, i.e., a Xe layer. This kind of experiment provides additional important information on the excitation mechanism.

Xenon in the first layer on Pt(111) showed a desorption peak at 109 K. With more extended Xe exposures TPD peaks from second and third layers developed at 72 and 65 K, respectively. The exposure of 12 L Xe at the surface temperature of 82 K was used to form a saturated monolayer of Xe. Then, methane was dosed to form an overlayer. The exposure of 1.6 L at 45 K saturated the first overlayer of methane. The peak temperature of methane desorption from this surface was 53 K. Thus, the CH_4/Xe/Pt(111) system is characterized by the two fingerprint TPD peaks recorded at $m/e=13$ (CH^+) and 131 (Xe^+).

The sample of CH_4/Xe/Pt(111) was irradiated with laser pulses (3 mJ cm^{-2} per pulse) of 6.4-eV photons up to $N_{\rm ph}=1.2\times10^{19}$ cm^{-2} at the surface temperature of 45 K (the lowest accessible at the time of experiment) and then post-irradiation TPD was carried out. The Xe-peak remained unchanged while the methane peak decreased by $\sim$10% of its area. However, no new peaks were detected. Since the desorption temperature of methane from the Xe overlayer is lower than from the bare surface, thermal desorption of weakly bound methane may be appreciable. To clarify this we evaluated a fraction of laser-induced thermal desorption by coupling a desorption rate constant of methane on the Xe overlayer and a time profile of surface temperature. The rate constant was obtained from the analysis of the methane desorption peak at 53 K and the time profile of the surface temperature was numerically calculated with the standard heat conduction model.[15] The fraction of thermal desorption appeared to be about 10% as detected in the experiment. Therefore, we conclude that *there is no photochemical activity of methane in the CH_4/Xe/Pt(111) system with the 6.4-eV photons.*

D. Photo-induced desorption

Photon irradiation leads not only to dissociation but also to desorption of adsorbates and their fragments. In order to obtain a deeper insight into the dynamics in the photochemistry of methane on Pt(111), we measured TOF distributions of desorbed species under the irradiation of 6.4-eV photons.

Both methane and methyl desorb from the surface. Figure 7 shows TOF distributions of desorbed species along the surface normal detected at $m/e=16$ (CH_4^+) and 15 (CH_3^+).

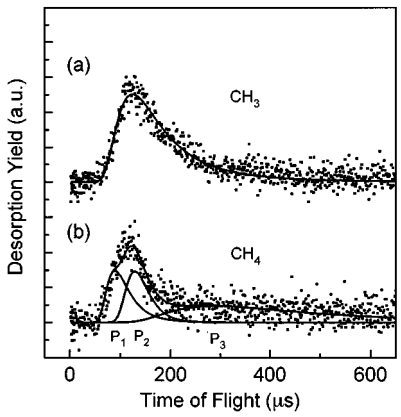

FIG. 7. Time-of-flight distributions of (a) CH_3 and (b) CH_4 desorbed from Pt(111) under the irradiation of 6.4-eV photons. $N_{ph}=3.0\times10^{19}$ cm^{-2} in (a) and 1.5×10^{18} cm^{-2} in (b). Desorbed species were detected along the surface normal. The contributions in the CH_3 TOF distribution from methane due to cracking of methane are subtracted by using the mass cracking pattern of CH_4 determined in separate measurements. Solid curves are the results of fitting to shifted Maxwell–Boltzmann velocity distributions.

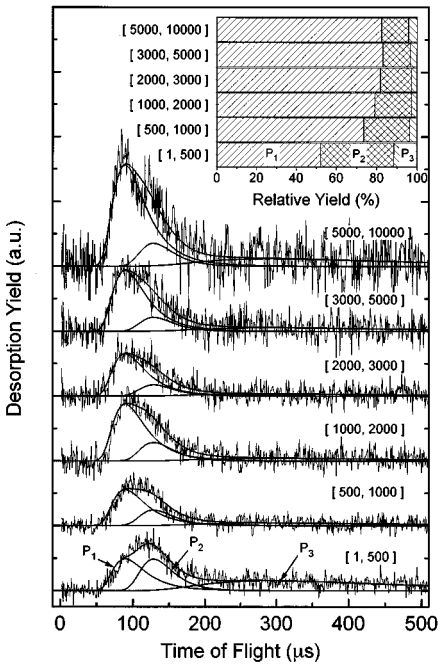

FIG. 8. Shot dependence of time-of-flight distributions of CH_4. The numbers in the bracket, $[n,m]$, denote that the desorption signals were accumulated in the interval from nth to mth laser pulses of 5 mJ cm^{-2}. Solid curves are results of fitting to three velocity components. The inset shows the relative contributions of the velocity components for each interval.

Since CH_4 contributes to the signals at $m/e=15$ via cracking in the ionizer of QMS, those contributions are subtracted from the raw data at $m/e=15$ by using the mass cracking pattern of CH_3 determined in separate measurements. The TOF distributions were fitted to a shifted Maxwell–Boltzmann velocity distributions of the functional form $f(v)=Av^3\exp[-(v-v_0)^2/B]$, where v_0 and B are the parameters representing the shift and spread in velocity, respectively. The TOF distribution of methyl was found to be close to the Maxwell–Boltzmann distribution with the average translational energy, $\langle E_T\rangle=0.27$ eV, i.e., $\langle E_T\rangle/2k=1550$ K. On the other hand, there are mainly two fast velocity components denoted as P_1 and P_2, followed by a slow component, P_3, in the TOF distribution of methane. The high average translational energies of the two fast components clearly indicate that nonthermal processes take place under the irradiation of 6.4-eV photons. On the other hand, the P_3 component is much slower. Thus, this component could be due to desorption of methane accommodated with the surface to some extent. Therefore, we focus on the two fast components for discussion on the dynamics of photodesorption.

Figure 8 shows a series of TOF distributions of methane. The numbers in the bracket, $[n, m]$, in the figure denote that desorption signals were accumulated in the interval from nth to mth laser pulses of 5 mJ cm^{-2} per pulse. It is evident particularly in the early stage (small number of laser shots) that three velocity components contribute to the TOF distributions. All of the TOF distributions were fitted simultaneously to three shifted Maxwell–Boltzmann velocity distribution functions, which resulted in $\langle E_T\rangle=0.53$ eV for P_1 and 0.26 eV for P_2, 0.057 eV, for P_3. As shown in the inset, while the relative contribution of the P_2 component decreases with the number of laser shots, that of the P_1 component increases.

The two fast velocity components in the methane TOF distributions along the surface normal are more prominent when desorption angles are increased. Figure 9 shows the desorption-angle dependence of TOF distributions. Here, we used CD_4 instead of CH_4 and measured TOF distributions of CD_4 at $m/e=20$, since smaller background signals enabled us to measure TOF distributions at much smaller levels of desorption signals particularly at off-normal angles. The P_1 and P_2 components are clearly seen at off-normal desorption angles. This indicates that the angular distributions of the two components are different. The TOF distributions of CD_4 were also fitted to shifted Maxwell–Boltzmann velocity distributions. The average translation energy of each component was not significantly dependent on the desorption angle. In addition, the angular distributions of the two components were obtained by fitting velocity-weighted integration of the TOF distributions per unit irradiated surface area to the functional form of $\cos^n\theta_{\rm des}$. The fitting procedures yielded the following results: $\langle E_T\rangle=0.53$ eV and $\cos^{62}\theta_{\rm des}$for P_1 and $\langle E_T\rangle=0.21$ eV and $\cos^{28}\theta_{\rm des}$ for P_2.

There are a couple of plausible origins for the two fast velocity components in the TOF distributions. First, two different adsorption states of methane may give rise to the two velocity components, since the quenching rate of an excited state may be sensitive to interactions between methane and substrate. However, the results of TPD, XPS, and IRAS (Ref. 7) do not show marked evidence for the two different adsorption states. Thus, it is not likely that different adsorption states reflect on the two fast components in TOF distributions. Second, inelastic collisions of desorbing methane with neighboring adsorbates may provide the P_2 component.

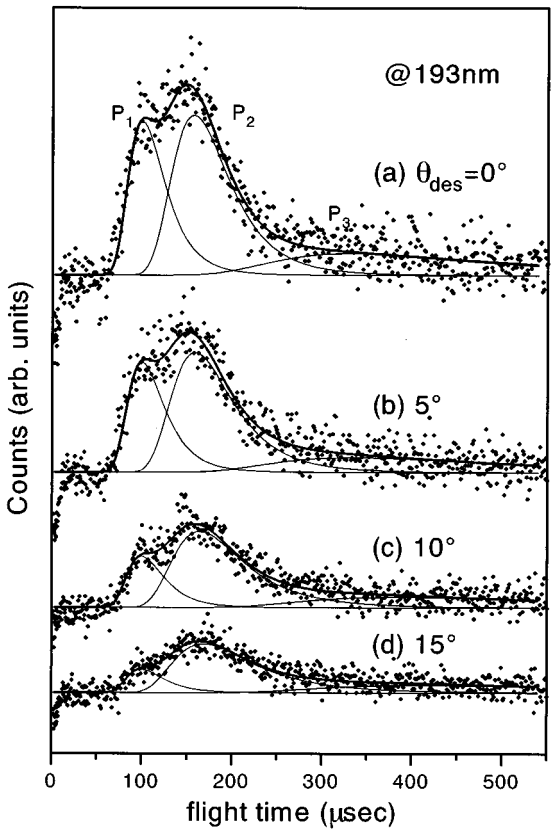

FIG. 9. Time-of-flight distributions of CD_4 from Pt(111) as a function of the desorption angle. (a) 0° (along the surface normal), (b) 5°, (c) 10°, (d) 15°. The surface was saturated with CD_4 and irradiated with 6.4-eV photons. Signals were detected at $m/e=20$ (CD_4^+).

Since this energy loss process would be effective at high adsorbate coverage, this mechanism could also explain the shot dependence of the TOF distributions. However, since methyl adsorbates produced by methane dissociation occupy almost similar space as methane at the surface, the effective adsorbate coverage including methane and methyl decreases only by ~12% of the initial methane coverage owing to methane and methyl desorption. Furthermore, the angular distribution of the P_2 component seems to be too sharp for the energy dissipation process. Thus, this energy loss mechanism may explain why the P_3 component appears, but is not responsible for the two fast components.

Another plausible origin of the two fast components may be due to photo-induced reactions between photofragments and adsorbed species. While desorption signals of CD_4 are accumulated, the coverage of CD_3 increases with laser shots up to 0.14 ML. Photodissociation of CD_4 produces CD_3 and D with excess energy. These fragments dissipate their excess energies and are finally trapped in chemisorption potential wells owing to strong interactions with the substrate atoms. However, these fragments may also react with coadsorbed species before they are completely accommodated at the surface. In fact, the hydrogenation of methyl photofragments was reported in the study of photodissociation of CH_3Br on Pt(111).[28] The other example of this type of photo-induced reaction is the oxygen combination reaction between an energetic oxygen atom produced by N_2O photodissociation on Pt(111) and a chemisorbed oxygen adatom.[29] Thus, CD_4 can be produced by the following reaction schemes:

$$CD_3^* + D(ad) \rightarrow CD_4(g), \tag{5}$$

$$D^* + CD_3(ad) \rightarrow CD_4(g). \tag{6}$$

Here, $CD_3^*(D^*)$ denotes a methyl radical (deuterium atom) in the transition between the adsorbed and the gaseous state.

In order to examine this possibility, we have performed the following measurements. First, CD_4 was adsorbed on the surface precovered with 1 ML of H atoms. Post-irradiation TPD showed that CD_4 is dissociated on the coadsorbed surface.[27] Attempts were made to detect CD_3H desorption under 6.4-eV photon irradiation, but signals of CD_3H ($m/e=19$) were below the detection limit. Thus, CD_3^* is not likely to react with neighboring deuterium adatoms. Second, the surface saturated with CD_4 was irradiated with a desired number of 6.4-eV photons and then annealed to 80 K. This procedure served to make 0.05 ML of CD_3 and D on the surface. After CH_4 was saturated on this surface, CD_3H desorption was measured upon the irradiation of 6.4-eV photons. In this case the desorption signals of CD_3H were detected and its TOF distribution was obtained as shown in the trace (a) in Fig. 10. The leading edge of the TOF distribution is very similar to that in the TOF distributions of CD_4. Therefore, these results strongly suggest that the P_1 component in the TOF distributions of CD_4 is attributable to the photo-induced reaction given by Eq. (6), but not to Eq. (5).

E. Polarization dependence

In order to obtain a clue for the excitation mechanism, we measured the polarization-dependent photochemical cross section as a function of the incident angle, γ. This technique has been used in quite a few systems and reviewed in detail.[2] The preliminary results on the present adsorption system have been reported in the previous paper.[12]

Figure 11 depicts experimental configurations used in the measurements. The incident laser beam was polarized either parallel (p-polarization) or perpendicular (s-polarization) to the plane of incidence. If a photochemical process is induced by the substrate-mediated excitation, the cross section of the process, $\sigma_j(j=p,s)$, depends on the number of hot carriers generated via photon absorption by the substrate. Thus, the cross section will be scaled with the polarization dependence of light absorbance of the substrate, A_j. On the other hand, if the process is induced by the direct excitation, the cross sections will be proportional to $|\boldsymbol{\mu}\cdot\mathbf{E}|^2$, where $\boldsymbol{\mu}$ is the transition dipole moment of adsorbate fixed to the adsorbate frame and $\mathbf{E}$ is the electric field vector at the surface boundary. Since the adlayer thickness is substantially small for a monolayer-covered metal surface, effects of the adlayer on the light reflection and refraction are negligible.[30]

Both light absorbance by metal substrates and mean square electric field strengths at surfaces can be evaluated by Fresnel's equations as shown in Fig. 12. Here, the refractive index of platinum at 193 nm ($n=1.32$ and $k=1.28$) (Ref. 31)

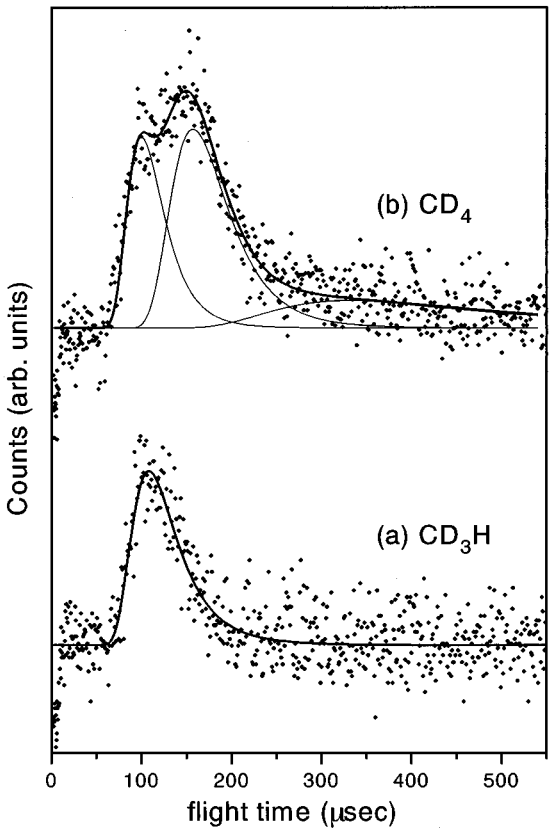

FIG. 10. Time-of-flight distributions of (a) CD_3H ($m/e=19$) from the coadsorbates of CD_3, D, and CH_4 on Pt(111) and (b) CD_4 ($m/e=20$) from the surface saturated with CD_4 under irradiation of 6.4-eV photons. Signals were detected along the surface normal. Note that the leading edge of the TOF distribution in (a) is very similar to that in (b).

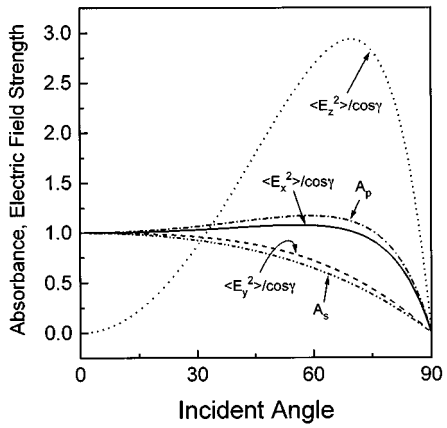

FIG. 12. Dependence of the electric field strengths and substrate absorbance on the incident angle for *p*- and *s*-polarized light ($\lambda=193$ nm) impinging on a platinum surface. The results are calculated from Fresnel's equations with the refractive index of $n=1.32$ and $k=1.28$ (Ref. 31).

was used in the calculations. The electric field strengths are divided by cos γ, since this correction factor is necessary when calculated results are directly compared with experimental ones normalized to the intercepted irradiance,[32] which was neglected in previous studies.[33–35] Note that γ-dependence of A_p and A_s resembles that of $\langle E_x^2\rangle/\cos\gamma$ and $\langle E_y^2\rangle/\cos\gamma$, respectively. Thus, as pointed out by Richter *et al.*,[32] it is practically impossible to distinguish between the two excitation mechanisms if the transition dipole moment lies in the plane parallel to the surface. Distinction between the two mechanisms can be made with this method only if adsorbed molecules have a nonzero component of the transition dipole moment perpendicular to the surface plane, $\mu_\perp$.

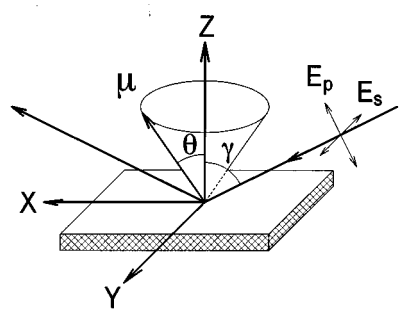

FIG. 11. Experimental configuration used in the measurements for incident angle dependence of cross sections with linearly polarized laser beams. The incident angle of linearly polarized laser is γ and a transition dipole moment is oriented along the polar angle of θ.

Although methane adsorbs on Pt(111) weakly, the symmetry of the adsorbate is reduced to at least C_{3v} from the T_d symmetry of gaseous methane according to IRAS measurements.[7] Thus, we assume that transition dipoles are not distributed isotropically, but rather oriented in such a way that they possess the same or higher rotational symmetry of the substrate, i.e., $\geqslant C_3$. In this case the cross sections can be described as,[2,36]

$$\sigma_p \propto [0.5\sin^2\theta\langle E_x^2\rangle + \cos^2\theta\langle E_z^2\rangle]/\cos\gamma, \tag{7}$$

$$\sigma_s \propto [0.5\sin^2\theta\langle E_y^2\rangle]/\cos\gamma, \tag{8}$$

where θ is a tilting angle of the transition dipole moment with respect to the surface normal.

In most of the previous works using this method, photochemical yields, Y_i $(i=p,s)$, were measured as a function of γ at *a fixed* $N_{\rm ph}$ for the impinging laser beam with *p*- and *s*-polarization. The ratio between the yields at each γ was often taken for comparison with calculated results, since taking the ratio serves to reduce systematic errors due to the changing geometrical arrangement and instrument variations.[34] We have not followed these procedures because of the following reasons. The validity of these procedures stands on the approximation of $Y_i \propto 1-\exp(-\sigma_i N_{\rm ph}) \approx \sigma_i N_{\rm ph}$, which is valid only if the yields are small, i.e., $\sigma_i N_{\rm ph} \ll 1$. Measuring the small yields causes erroneous results owing to poor S/N ratios and pulse-to-pulse fluctuations of laser fluence, etc. Although irradiation with a large number of photons gives reasonable changes in post-irradiation TPD, the linear approximation becomes inappropriate. Furthermore, the photochemistry of the present adsorption system is self-quenched at $N_{\rm ph}\sim 2\times 10^{19}$ cm^{-2}. Thus, we instead repeated post-irradiation TPD measurements as a function of $N_{\rm ph}$ at various incident angles for *p*- and *s*-polarization to

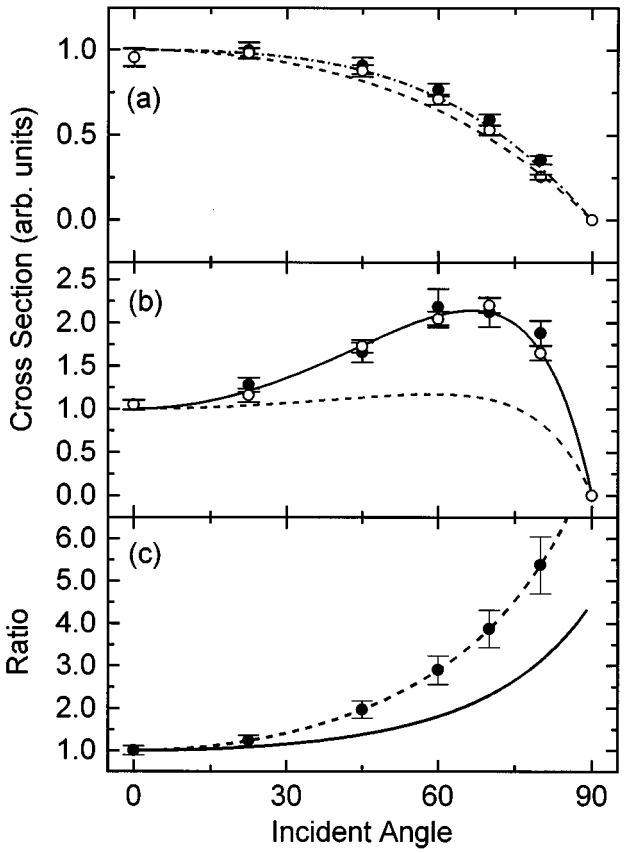

FIG. 13. Incident-angle (γ) dependence of photochemical cross sections determined by using the α (solid circles) and the β (open circles) desorption peaks in post-irradiation TPD with various numbers of photons incident on the surface. The impinging light was polarized (a) perpendicular (s-polarization) and (b) parallel (p-polarization) to the plane of incidence. The dashed curves in (a) and (b) are calculated absorbance of the platinum substrate. The dashed–dotted curve in (a) is $\langle E_y^2 \rangle / \cos \gamma$. The solid curve in (b) represents the best fitting result to Eq. (7), resulting $\theta = 66°$ at $|e_{\text{eff}}| = 1$. (c) The ratios of the cross sections obtained from the measurements with p-polarization to those with s-polarization. The solid and the dashed curves in (c) represent the ratio of A_p/A_s and that of cross sections based on the calculations by Eqs. (7) and (8) with $\theta = 66°$, respectively.

obtain the cross sections from the α- and the β-desorption peaks independently as described in Sec. III B.

The cross section estimated from the α desorption peak is larger than that from the β-desorption peak by 55% in each set of measurements. The cross sections are normalized at $\gamma = 0°$ and plotted as a function of γ in Fig. 13. Figure 13(a) shows that the γ-dependence of σ_s agrees quite well with the calculated curves of A_s and σ_s depicted with the dashed and the dashed-dotted curves, respectively. Although the measurements with s-polarized light do not provide a critical test for distinction between the two excitation mechanisms, the satisfactory agreement between the experimental and the theoretical results encouraged us to perform measurements with p polarization with full confidence.

Figure 13(b) shows the γ-dependence of σ_p. Again, the results obtained from the two desorption peaks are normalized at $\gamma = 0°$. In contrast to the γ-dependence of σ_s, σ_p is peaked at $\gamma = 70°$. Note that it deviates significantly from A_p drawn by the dashed curve. The deviation is also confirmed by comparison of the ratios of σ_p to σ_s as shown in Fig. 13(c). These results clearly demonstrate that *the photochemical processes cannot be accounted for only by the substrate-mediated excitation; the direct excitation with the transition dipole component perpendicular to the surface must be taken into account.*

Equations (7) and (8) are derived from the macroscopic classical treatment of the electric field at the surface. The assumptions of a step-function for the electric field normal to the surface used in the macroscopic treatment is certainly not valid in a microscopic scale. Instead of a step function, the electric field normal to the surface is expected to change smoothly from E_z to E_z/ϵ_s, where ϵ_s is the dielectric constant of the substrate. However, exact calculations of the electric field strengths as a function of the distance from the platinum surface are not available. Thus, following the treatment done in previous works,[2,37] we describe the microscopic field as $E_z/\epsilon_{\text{eff}}$ at the vacuum side near the surface where adsorbates are located.

Calculations by Feibelman[38] based on a jellium model demonstrated that the macroscopic description is a reasonable approximation for distances greater than about 1 Å outside the jellium edge. In this approximation, i.e., $|\epsilon_{\text{eff}}| = 1$, the satisfactory fit to Eq. (7) drawn by the solid curve in Fig. 13(b) gives $\theta = 66°$; $|\mu_\perp| : |\mu_\parallel| \approx 4:9$. If the classical treatment cited above is not appropriate, $|\epsilon_{\text{eff}}|$ takes the value between 1 and $|\epsilon_s|$ (3.38 at 193 nm). Although the data of σ_p were fitted with two free parameters, $|\epsilon_{\text{eff}}|$ and θ, they could not be determined independently from the fitting. Thus, we set $|\epsilon_{\text{eff}}| = |\epsilon_s|$ as the other extreme case. The equally satisfactory fit was also obtained, resulting in $\theta = 34°$; $|\mu_\perp| : |\mu_\parallel| \approx 3:2$.

Although the present data clearly show that the direct excitation with the transition dipole moment perpendicular to the surface plays an important role in the photochemistry, it does not completely exclude the involvement of the surface-mediated excitation. Assuming that the photochemistry of methane is induced via both the direct and the indirect excitation mechanisms, we could also fit the experimental data by the combination of Eq. (7) with $\theta = 0°$ and A_p as equally well as the fits described in the preceding paragraph.

IV. DISCUSSION

A. Adsorbate–substrate interactions

Since methane is a closed-shell molecule with high symmetry, comparison with rare gas atoms on metal surfaces is useful for understanding the nature of methane–substrate interactions. Rare gas atoms on metal surfaces are prototype physisorption systems and their adsorption properties have been extensively studied.[39] There are two types of metal surfaces which show quite different behavior in work function changes induced by adsorption of rare-gas atoms. While work functions changes are small or almost zero at the saturation coverage for the metal surfaces with work functions near 2 eV, changes are large up to ~1 eV for those with work functions larger than 4 eV and the bonding energy of rare-gas atoms increases with the work function change.

There are some common features between methane on Pt(111) and rare gas atoms on the metal surfaces with $\phi \geqslant 4$ eV, such as Xe on tungsten. (1) The adsorption-induced work function changes are large ($-0.5 \sim -1.0$ eV) and the coverage dependence of $\Delta\phi$ is well described by the Topping model. This indicates that a large dipole is induced at low coverage, but mutual depolarization takes place at high coverage. (2) Heat of adsorption is larger than that of sublimation. If heat of sublimation is regarded as a measure of pure dispersion forces, this suggests that the interactions of the adsorbates with metal surfaces are stronger than pure dispersion forces. These properties could be attributed to large polarizabilities of the adsorbates. In fact, although the united atom of methane is Ne, the polarizability of methane is larger than that of Ne and almost equivalent to that of Kr. Thus, the ''soft'' electronic shell may easily become polarized on the metal surface. However, an exclusive operation of van der Waals forces cannot account for the rather large $\Delta\phi$ values. Therefore, some chemical interaction should be taken into account for the large work function change.

These interactions manifest themselves in the structural change of methane when it adsorbs on Pt(111). The structural information of methane on Pt(111) has been obtained by Yoshinobu *et al.*[7] in the IRAS study. While methane in the second layer retains T_d symmetry, methane in the first layer is deformed from T_d to C_{3v}, or lower symmetries. Therefore, the adsorption structure of methane in the first layer is clearly different from the one in the second layer and in the gas phase.

B. Excitation mechanisms

It is remarkable that methane on Pt(111) is dissociated at 193 nm, where there is no appreciable absorption cross section for methane in the gas phase. Since the dissociation of methane adsorbed on Pt(111) is not induced thermally, electronic excitation must be responsible for the photochemical process. The interaction strength of methane in the ground electronic state is small, i.e., 0.23 eV, thus, methane adsorption on Pt(111) is regarded as physisorption. However, this may not imply that methane in its electronically excited states also weakly interacts with surface atoms. If an orbital of the excited state is diffuse, this state would strongly interact with surface electronic states when the molecule is closely located at the metal surface. Therefore, it is necessary to consider the excited electronic state of the adsorbate–substrate complex as a whole. The detailed knowledge on electronic excited states of adsorbates is essential for understanding the excitation mechanism in surface photochemistry on metal and semiconductor surfaces. However, this is often unavailable. The system of methane on Pt(111) is not an exception. Thus, we are forced to speculate on the plausible excitation mechanism on the basis of the electronic structure of methane in the gas phase. The cross section measurements with polarized light described in Sec. III E provide direct evidence for the direct electronic excitation with a transition dipole component perpendicular to the surface. However, since the substrate-mediated excitation cannot be completely ruled out by the measurements, we discuss plausible excitation pathways in terms of both mechanisms.

The relevant electronic configurations of methane for the photochemical processes are the ground and the first excited states of neutral methane, and transient negative ion states. We first summarize the electronic structures of neutral methane in the gas phase. The electronic configuration for the ground state of methane is $(1a_1)^2(2a_1)^2(1t_2)^6$, $^1A_1$. The first excited state of methane in the gas phase, $(1t_2 \rightarrow 3sa_1^1)$, $^1T_2$, is located at $\sim$10 eV above the ground state. The excited-state orbital is essentially a $3s$ Rydberg-type orbital. The degenerate excited state is split into two states owing to Jahn–Teller distortion. Absorption peaks at 9.7 and 10.3 eV are assigned to the transitions to the excited state with D_{2d} and that with C_{3v} symmetry, respectively.[10] Excitation to the excited states leads to dissociation of methane to CH_2+H_2 and CH_3+H, which has been studied in experiments[10,40–44] and in theoretical calculations.[45–48]

Transient negative ion states of methane have been investigated by various methods including direct electron transmission spectroscopy, electron scattering, and dissociative attachment studies.[49] The resonance feature at around 10 eV of electron energy has been unambiguously assigned to the lowest Feshbach resonance, $(1t_2 \rightarrow 3sa_1^2)$ $^2T_2$. The transient negative ion state proceeds to dissociation to CH_3 and H^-. Below this electron energy the assignments of resonance features are not necessarily clear. However, these resonance features are all related to inelastic scattering, such as vibrational excitation, and no dissociative electron attachment were observed.

Electron scattering experiments on thin films of methane on metal surfaces also provide useful information on transient negative ion states. The resonance feature of the dissociative electron attachment was also found at 9.1 eV for monolayer of methane and 10.8 eV for multilayers on a polycrystalline platinum foil.[50] The study of electron transmission through solid methane films showed a sharp resonance at 2.5 eV.[51] Robin suggested[49] that the resonance in the low energy range is due to the transient negative ion resonance associated with $a_1\sigma^*$ $^2A_1$. Sanche and co-workers[52] have demonstrated that the lowest conduction band of methane thin films on Pt(111) is located from -0.2 to 2 eV relative to vacuum presumably along the (111) direction by analyzing interference features in electron transmission spectra.

The electronic structure of gaseous methane will be modified as a function of the distance between the adsorbate and the Pt(111) surface, z. The ground state of neutral methane has a shallow well near the surface, which is responsible for the adsorption of methane. Since the ionization potential of gaseous methane is 13 V and the work function of bare Pt(111) is 6 eV, the excited state of gaseous methane is located at 3 eV above the Fermi level at a far distance from the surface. In contrast to the ground state, the excited state with the $3s$ orbital character can be perturbed with electronic states of the substrate with decreasing z more extensively. As a result of the interactions, the excited state will be not only broadened but also shifted by hybridization with orbitals of

the substrate. The strong interactions in the excited state manifest themselves in the large red shift of >2 eV; while the onset of the absorption based of gasous methane[8–10] is 8.5 eV, the photochemistry of methane on Pt(111) readily occurs at 6.4 eV.

As mentioned earlier, the Jahn–Teller instability induces structural changes of gaseous methane in the first excited state from T_d to D_{2d} and C_{3v}. In addition, the interactions with substrate electronic states likely give rise to symmetry reduction of the adsorbate excited state as observed in the ground state. If the T_d symmetry is reduced to the lower symmetries, the excited state is split to $A_1+E(C_{3v})$ or $A_1+B_1+B_2(C_{2v})$, etc. Then, the allowed transitions for these cases are $A_1 \leftarrow A_1$ for $\mu_\perp$, $E(B_1,B_2) \leftarrow A_1$ for $\mu_\parallel$. Therefore, both of the transition to these excited states perpendicular and parallel to the surface are allowed; this accords qualitatively with the observed results.

The negative ion state of gaseous methane will be also modified with decrease of z. The energy of the negative ion state is lowered as $-e^2/4z$ by the image force when the ion is close to the metal surface. The stabilization energy is estimated to be -1.57 eV at $z=2$ Å (van der Waals radius of methane). Polarization of the surrounding adsorbates and chemical bonding/antibonding interactions between the negative ion state and its surroundings also cause the energy shift.[53] According to Sanche and co-workers,[50] the DEA resonance energy of methane on a polycrystalline platinum foil shifts from 10.8 to 9.1 eV as the methane film proceeds from multilayers to monolayer. The observed shift is comparable to the stabilization energy due to the image force, but far insufficient to bring the negative ions state into the energy accessible for energetic electrons associated with substrate absorption of 6.4-eV photons. Thus, it is unlikely that the excited state of the adsorbate correlating with the $^2T_2$ state can be accessed by 6.4-eV photons. On the other hand, the negative ion state correlating with the lowest conduction band observed in thin films may be accessible, since the energy of the band around 1 eV with respect to vacuum is low enough compared with the DEA state. Although low energy electrons injected in the conduction band of the methane film only suffer from elastic scattering, they might induce dissociation of monolayer methane as a result of specific chemical interactions between the negative ion state with substrate electronic states. However, we think that this is not likely either for the following reason. Since the low-lying negative ion state would also be stabilized by the image force and so forth as described above, this state could be accessible even with 5.0-eV (248 nm) photon irradiation. However, no photochemical processes have been observed at 248 nm. Consequently, the low-lying negative ion state is not likely involved in the photochemistry of methane on Pt(111).

Since electrons in a surface state of metal substrate are localized near the surface, the electronic excitation from the surface state to an adsorbate unoccupied state is another possible excitation mechanism in surface photochemistry. The surface state of Pt(111) is located at ~0.4 eV below the Fermi level.[54] This was identified by comparison of angle-resolved ultraviolet photoemission spectra of clean Pt(111) with those of an O-atom precovered surface. Thus, the surface state is quenched on the O-precovered surface. To examine this excitation path we have performed the following measurements.[55] Methane was adsorbed on a 0.25 ML O-precovered Pt(111) surface and irradiated with 6.4-eV photons. If the excitation from the surface state to the unoccupied state of methane were responsible for the photochemistry, we would expect no photochemistry of methane on the O-precovered surface, provided that the surface state is completely quenched by the oxygen adatoms. However, post-irradiation TPD showed that a strong CO_2 desorption peak at 405 K, indicating that methane can also be dissociated on the O-precovered surface and further oxidized in the annealing process. Therefore, it is not likely that the surface state (if any) at methane-covered Pt(111) is involved in the excitation.

In conclusion, we believe that the excitation from the adsorbate-localized orbital to the excited stat of methane significantly mixed with substrate electronic states plays a major role in the photochemistry of methane on Pt(111).

C. Comparison with other systems

It is interesting to compare the photodissociation of methane with other adsorption systems where direct excitation is believed to be responsible for their photochemistry. Ho and co-workers[37,56,57] demonstrated that direct excitation plays a major role in photodissociation of $Mo(CO)_6$ physisorbed on various substrates above 250 nm. The direct excitation in the photochemistry of weakly adsorbed $Mo(CO)_6$ on various surfaces was confirmed from the close resemblance of the wavelength dependence of the photodissociation yield to that of optical absorption measured in cyclohexane. Electronic excitations involved above 250 nm are the ligand-field transition ($4d \rightarrow 4d^*$) and the metal-to-ligand charge transfer transition ($4d \rightarrow 2\pi^*$) of $Mo(CO)_6$. Negligible shifts in the photo-yield spectra imply that these excited states of $Mo(CO)_6$ interact very weakly with substrate electronic states as the ground state of the adsorbate.

Another example is photodissociation of phosgene (Cl_2CO) on Pt(111) and Pd(111) studied by White and co-workers.[5,58] They showed that the similar deviations in the incident angle dependence of photodissociation yields of phosgene on these surfaces for p-polarized light at 248 nm and 280 nm and concluded that both the direct and the substrate-mediated excitations take place. Phosgene is also weakly held on Pt(111). Photodissociation cross sections of phosgene on Pt(111) rapidly increases between 305 and 250 nm, which accords with the wavelength dependence of the optical absorption cross section in the gas phase. It is known that phosgene is photodissociated to COCl and Cl at the wavelengths.[59] Thus, the excited state involved in the photodissociation would not be severely perturbed as $Mo(CO)_6$.

In contrast, methane on Pt(111) is photochemically active at 193 nm, where gaseous methane is transparent and no photochemistry takes place. The involvement of the direct excitation implies the strong mixing with substrate electronic states in the excited state of the methane–substrate complex.

The difference from the adsorption systems cited above could be due to the specific nature of the σ^* antibonding valence orbital of methane that is completely miscible with dense diffuse Rydberg levels. This strong interaction with substrate in the excited state may cause rapid quenching of the excited state. However, C–H bond rupture can compete with the quenching owing to a rapid motion of hydrogen on the repulsive PES in the excited state.

D. Reaction scheme and quenching of the photochemical processes

According to the results presented above, photo-induced processes of methane on Pt(111) are summarized as follows:

$$CH_4(\mathrm{ad}) + h\nu \rightarrow CH_3^* + H^*, \tag{9}$$

$$CH_4(\mathrm{ad}) + h\nu \rightarrow CH_4(g), \tag{10}$$

$$CH_3^* \rightarrow CH_3(\mathrm{ad}), \tag{11}$$

$$CH_3^* \rightarrow CH_3(g), \tag{12}$$

$$H^* \rightarrow H(\mathrm{ad}), \tag{13}$$

$$H^* \rightarrow (H)(g), \tag{14}$$

$$H^* + CH_3(\mathrm{ad}) \rightarrow CH_4(g), \tag{15}$$

$$CH_3^* + H(\mathrm{ad}) \rightarrow CH_4(\mathrm{ad}). \tag{16}$$

Although not mentioned here, a very minor channel in Eq. (16) was reported in the study of photochemistry of methane on hydrogen precovered Pt(111).[27] Thus, these reactions are confirmed experimentally except for the ejection of H in Eq. (14) that is difficult to detect with the detection method of this study because of the large background signals of H^+ at the QMS ionizer. The loss mechanisms of methane adsorbates include photodissociation in Eq. (9) and photodesorption in Eq. (10). Thus, the cross section obtained from the α desorption peak accounts for the total depletion of methane adsorbates due to the two processes. On the other hand, since there are the loss mechanisms of methyl adsorbates including photoejection in Eqs. (9) and (12) and photo-induced associative recombination in Eqs. (15) and (16), the cross section obtained from the β-desorption peak is smaller than the one from the α-desorption peak, as described in Sec. III B.

We discuss why the β-desorption peak apparently levels off at around 0.14 ML of the methyl coverage. Since hydrogen atoms produced via the dissociation of adsorbed methane react with CH_3(ad), the coverage of methyl could be steady if the production rate via Eqs. (9) and (11) is balanced to the annihilation rate via Eq. (15). This balancing would be accomplished at large N_{ph}, since the annihilation rate is large when the coverage of methyl is large. This is evidently observed as shown in Fig. 8; the shot dependence of TOF distributions of methane reveals that the relative contribution of the P_1 component due to photo-induced associative desorption in Eq. (15) increases with N_{ph}. Furthermore, the production rate of methyl adsorbate significantly slows down at prolonged irradiation owing to the self-quenching mechanism. This also helps to keep the coverage of methyl constant.

The quenching of the photochemical processes could be understood if the excitation itself becomes forbidden. Yoshinobu *et al.*[7] have reported that methane adsorbed on Pt(111) covered with methyl and hydrogen retains T_d symmetry. This finding suggests that the adsorbate–substrate interactions become weaker as the photodissociation of methane proceeds. In the saturation region the interactions are not strong enough to alter the structure of methane. However, note that the change in the interaction strength is not large if one compare the TPD spectra before and after irradiation (Fig. 3); the shift in the peak temperature of the molecular desorption is only 5 K. Thus, we believe that the methane adsorbates in the saturation region are still in the first layer and directly interact with metal atoms, but the distance from the surface is slightly elongated owing to repulsive interactions with surrounding adsorbates. This is reasonable because the surface is more congested with methyl and hydrogen adsorbates. Although the difference is subtle, this may reduce excitation probability significantly if the longer distance from the metal surface prevents the excited state of the adsorbate from significant mixing with the substrate electronic states.

V. CONCLUSION

We have shown that methane adsorbed on Pt(111) undergoes nonthermal processes such as desorption and dissociation into methyl and hydrogen upon the irradiation of 6.4-eV photons. However, no nonthermal processes take place with 5.0-eV photon irradiation. Even with 6.4-eV photons methane adsorbed on a Xe overlayer is inactive. The photochemical reaction rate is strongly reduced when the surface becomes congested with methyl and hydrogen photoproducts. This is interpreted as the result of a slight increase in the methane–surface distance due to the repulsive force from surrounding adsorbates. Therefore, it is very crucial that methane has to be in close contact with surface platinum atoms for these photochemical processes to occur.

Most photofragments remain on the surface after 6.4-eV photon irradiation. However, some fraction of methyl fragments desorbs with a high kinetic energy. Desorption of methane is also observed. Desorbed methane has two nonthermal velocity components with narrow angular distributions along the surface normal. We identified that the faster component arises from recombination of methyl adsorbate with an energetic hydrogen atom produced by photodissociation of adsorbed methane.

Electronic excitation must be responsible for the photochemical processes. Incident angle dependence of cross sections measured with linearly polarized light clearly indicates that the direct electronic transition with a transition dipole moment perpendicular to the surface plays an important role in the photochemistry. The photochemistry observed with 6.4-eV photons strongly suggests that methane in an electronic excited state interacts substantially with substrate elec-

tronic states to form the excited electronic state of the complex of methane–platinum substrate atoms. If methane is located close to the metal surface, the interactions are strong enough to bring about the transition to the excited state by the 6.4-eV photon. This is why a close proximity to the metal surface is required for the photochemical processes. The strong mixing in the electronic excited state manifests itself in a couple of adsorption properties such as a large dipole moment of 0.54 D and the structural deformation of methane in the first layer from T_d to the lower symmetries such as C_{3v}, C_{2v}, etc.

ACKNOWLEDGMENTS

This work was supported in part by Grants-in-Aid for Scientific Research (06453030, 06228232 and 06NP0301) from the Ministry of Education, Science, Sports and Culture of Japan. Y.A.G. gratefully acknowledges the Japan Society for the Promotion of Science for a postdoctoral fellowship. We are grateful to M. C. Lin, J. C. Polanyi, and X.-Y. Zhu for fruitful discussions and to J. Yoshinobu and M. Kawai for providing the IRAS results prior to publication.

[1] X.-Y. Zhu, Annu. Rev. Chem. Phys. **45**, 112 (1994).
[2] X.-L. Zhou, X.-Y. Zhu, and J. M. White, Surf. Sci. Rep. **13**, 73 (1991).
[3] J. C. Polanyi and H. Rieley, *Dynamics of Gas–Surface Interactions*, edited by C. T. Rettner and M. N. R. Ashfold (The Royal Society of Chemistry, Cambridge, 1991), p. 329.
[4] W. Ho, *Laser Spectroscopy and Photochemistry on Metal Surfaces*, edited by H.-L. Dai and W. Ho (World Scientific, Singapore, 1995), Part 2, Chap. 24, pp. 1047–1140.
[5] X.-L. Zhou and J. M. White, *Laser Spectroscopy and Photochemistry on Metal Surfaces*, edited by H.-L. Dai and W. Ho (World Scientific, Singapore, 1995), Part 2, Chap. 25, pp. 1141–1240.
[6] Y. A. Gruzdkov, K. Watanabe, K. Sawabe, and Y. Matsumoto, Chem. Phys. Lett. **227**, 243 (1994).
[7] J. Yoshinobu, H. Ogasawara, and M. Kawai, Phys. Rev. Lett. **75**, 2176 (1995).
[8] R. W. Ditchburn, Proc. R. Soc. London Ser. A **229**, 44 (1955).
[9] N. Wainfan, W. C. Walker, and G. L. Weissler, Phys. Rev. **99**, 542 (1955).
[10] L. C. Lee and C. C. Chiang, J. Chem. Phys. **78**, 688 (1983).
[11] T. E. Sharp and J. T. Dowell, J. Chem. Phys. **46**, 1530 (1967).
[12] K. Watanabe, K. Sawabe, and Y. Matsumoto, Phys. Rev. Lett. **76**, 1751 (1996).
[13] K. Sawabe and Y. Matsumoto, Chem. Phys. Lett. **194**, 45 (1992).
[14] K. Sawabe and Y. Matsumoto, Surf. Sci. **283**, 126 (1993).
[15] R. B. Hall, J. Phys. Chem. **91**, 1007 (1987).
[16] D. L. Meixner and S. M. George, Surf. Sci. **297**, 27 (1993).
[17] V. A. Ukraintsev and I. Harrison, Surf. Sci. Lett. **286**, L571 (1993).
[18] A. C. Luntz and D. S. Bethune, J. Chem. Phys. **90**, 1274 (1989).
[19] J. Harris, J. Simon, A. C. Luntz, C. B. Mullins, and C. T. Rettner, Phys. Rev. Lett. **67**, 652 (1991).
[20] E. Habenschaden and J. Küppers, Surf. Sci. Lett. **138**, L147 (1984).
[21] H. Steininger, S. Lehwald, and H. Ibach, Surf. Sci. **123**, 264 (1982).
[22] K. Griffiths, W. N. Lennard, I. V. Mitchell, P. R. Norton, G. Pirug, and H. P. Bonzel, Surf. Sci. Lett. **284**, L389 (1993).
[23] J. Topping, Proc. R. Soc. London A **114**, 67 (1927).
[24] F. Zaera and H. Hoffmann, J. Phys. Chem. **95**, 6297 (1991).
[25] M. E. Pansoy-Hjelvik, R. Xu, Q. Gao, K. Weller, F. Feher, and J. C. Hemminger, Surf. Sci. **312**, 97 (1994).
[26] D. H. Fairbrother, X. D. Peng, R. Viswanathan, P. C. Stair, M. Trenary, and J. Fan, Surf. Sci. Lett. **285**, L455 (1993).
[27] Y. A. Gruzdkov, K. Watanabe, and Y. Matsumoto, Surf. Sci. **363**, 195 (1996).
[28] V. A. Ukraintsev and I. Harrison, J. Chem. Phys. **98**, 5971 (1993).
[29] K. Sawabe, J. Lee, and Y. Matsumoto, J. Chem. Phys. **99**, 3143 (1993).
[30] J. D. E. McIntyne, *Advances in Electrochemistry and Electrochemical Engineering*, edited by P. Delahay and C. W. Tobias (Wiley, New York, 1973), Vol. 9, p. 61.
[31] *Handbook of Optical Constants of Solids*, edited by E. D. Palik (Academic, Orlando, 1985).
[32] L. J. Richter, S. A. Buntin, D. S. King, and R. R. Cavanagh, Chem. Phys. Lett. **186**, 423 (1991).
[33] X.-Y. Zhu, S. R. Hatch, A. Campion, and J. M. White, J. Chem. Phys. **91**, 5011 (1989).
[34] E. Hasselbrink, S. Jakubith, S. Nettesheim, M. Wolf, A. Cassuto, and G. Ertl, J. Chem. Phys. **92**, 3154 (1990); M. Wolf, E. Hasselbrink, J. M. White, and G. Ertl, *ibid*. **93**, 5327 (1990); M. Wolf, E. Hasselbrink, G. Ertl, X.-Y. Zhu, and J. M. White, Surf. Sci. **248**, L235 (1991).
[35] S. A. Buntin, L. J. Richter, D. S. King, and R. R. Cavanagh, J. Chem. Phys. **91**, 6249 (1989).
[36] X.-Y. Zhu, J. M. White, M. Wolf, E. Hasselbrink, and G. Ertl, Chem. Phys. Lett. **176**, 459 (1991).
[37] Z. C. Ying and W. Ho, J. Chem. Phys. **94**, 5701 (1991).
[38] P. J. Feibelman, Prog. Surf. Sci. **12**, 287 (1982).
[39] See, for example, Y. C. Chen, J. E. Cunningham, and C. P. Flynn, Phys. Rev. B **30**, 7317 (1984), and references therein.
[40] B. H. Mahan and R. Mandal, J. Chem. Phys. **37**, 207 (1962).
[41] A. H. Laufer and J. R. McNesby, J. Chem. Phys. **49**, 2272 (1968).
[42] R. E. Rebbert and P. Ausloos, J. Photochem. **1**, 171 (1972/73).
[43] A. R. Welch and D. L. Judge, J. Chem. Phys. **57**, 286 (1972).
[44] T. G. Slanger and G. Black, J. Chem. Phys. **77**, 2432 (1982).
[45] S. Karplus and R. Bersohn, J. Chem. Phys. **51**, 2040 (1969).
[46] H. U. Lee and R. Janoschek, Chem. Phys. **39**, 271 (1979).
[47] M. S. Gordon, Chem. Phys. Lett. **44**, 507 (1976).
[48] M. S. Gordon and J. W. Caldwell, J. Chem. Phys. **70**, 5503 (1979).
[49] M. B. Robin, *Higher Excited States of Polyatomic Molecules* (Academic, London, 1985), Vol. 3, p. 82.
[50] P. Rowntree, L. Parenteau, and L. Sanche, J. Phys. Chem. **95**, 4902 (1991).
[51] T. Huang and W. H. Hamill, J. Phys. Chem. **78**, 2077 (1974).
[52] G. Perluzzo, G. Bader, L. G. Caron, and L. Sanche, Phys. Rev. Lett. **55**, 545 (1985).
[53] V. A. Ukraintsev, T. J. Long, and I. Harrison, J. Chem. Phys. **96**, 3957 (1992).
[54] P. Roos, E. Bertel, and K. D. Rendulic, Chem. Phys. Lett. **232**, 537 (1995).
[55] Y. Matsumoto (unpublished).
[56] Z. C. Ying and W. Ho, J. Chem. Phys. **93**, 9077 (1990).
[57] S. K. So and W. Ho, J. Chem. Phys. **95**, 656 (1991).
[58] X.-Y. Zhu and J. M. White, J. Chem. Phys. **94**, 1555 (1991).
[59] H. Okabe, *Photochemistry of Small Molecules* (Wiley, New York, 1978), pp. 289–291, and references therein.